

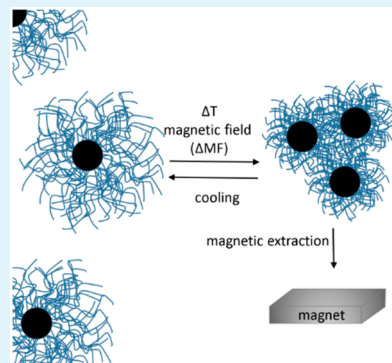
Synthesis and Magneto-Thermal Actuation of Iron Oxide Core–PNIPAM Shell Nanoparticles

Steffen Kurzhals, Ronald Zirbs, and Erik Reimhult*

Institute for Biologically Inspired Materials, Department of Nanobiotechnology, University of Natural Resources and Life Sciences, Vienna, Muthgasse 11, A-1190 Vienna, Austria

Supporting Information

ABSTRACT: Superparamagnetic nanoparticles have been proposed for many applications in biotechnology and medicine. In this paper, it is demonstrated how the excellent colloidal stability and magnetic properties of monodisperse and individually densely grafted iron oxide nanoparticles can be used to manipulate reversibly the solubility of nanoparticles with a poly(*N*-isopropylacrylamide)-nitrodopamine shell. “Grafting-to” and “grafting-from” methods for synthesis of an irreversibly anchored brush shell to monodisperse, oleic acid coated iron oxide cores are compared. Thereafter, it is shown that local heating by magnetic fields as well as global thermal heating can be used to efficiently and reversibly aggregate, magnetically extract nanoparticles from solution and spontaneously redisperse them. The coupling of magnetic and thermally responsive properties points to novel uses as smart materials, for example, in integrated devices for molecular separation and extraction.



KEYWORDS: iron oxide nanoparticles, responsive PNIPAM brush, core–shell nanoparticles, magnetic heating, polymer shell grafting

INTRODUCTION

Iron oxide nanoparticles have found widespread use in the biomedical field as well as for biotechnological applications. They are already in commercial use as contrast agents and as part of biomolecule extraction and purification systems;^{1–3} their uses in biosensors and for drug delivery are under increasingly intense development.^{3,4} A crucial point for all biomedical and biotechnological applications is the ability to disperse the nanoparticles and to control their state of aggregation. Most often, a highly solvated polymer brush is used to suspend nanoparticles, which for pharmaceutical applications almost exclusively is PEG or dextran.¹ The formed can be grafted to the particle surface; however, the latter is used as a physisorbed shell around the particle cores which yields poor control over surface and colloidal properties.

Poly-*N*-isopropylacrylamide (PNIPAM) brushes are interesting alternatives to form the hydrophilic polymer shell around the iron oxide core and their introduction could open up a large range of new applications. For example, a PNIPAM brush shell allows dispersion of superparamagnetic iron oxide nanoparticles in aqueous medium, but it could also allow for reversible aggregation and dispersion due to its drastic change in solvation at ~32 °C. This lower critical solution temperature (LCST) for PNIPAM was first described by Heskins and Guillet.⁵ Reversible temperature-induced aggregation at biologically relevant temperatures of well-dispersed particles is useful for many diverse applications,⁶ e.g., for drug delivery,^{7,8} self-healing materials, sensors and self-tuning catalysts,⁶ synthetic cells and organelles,^{9,10} efficient separation of NPs, emulsions and captured ligands^{6,11–13} or as building blocks in responsive

membranes.¹⁴ The latter two are interesting novel technologies for molecular separation and fishing. Although the biocompatibility of PNIPAM for in vivo applications is still in question, biotechnological applications only require that the particles can perform their function in various molecularly and colloidally complex environments.

Superparamagnetic iron oxide cores, which have diameters below 15 nm, are individually not easily translocated or extracted from solution by a magnetic field gradient. The field of even a lab-type permanent magnet is not sufficient for this purpose. Stabilization of individual particles by a PNIPAM shell is in light of this particularly interesting; such particles could (a) be easily and stably dispersed in, e.g., a biofluid, (b) be separated by magnetic fields after temperature induced aggregation,¹¹ which increases the effective magnetic particle size, and (c) the aggregation could be induced by local magnetic heating in alternating magnetic fields^{14–17} without direct change of the global temperature. Making use of increasingly sophisticated and precisely controlled iron oxide core–PNIPAM shell nanoparticles, such possibilities have started to be investigated. For example, Lu and co-workers showed that magnetic nanoparticles coated by copolymers including PNIPAM blocks could be used as draw solution for desalination where the nanoparticles later were partly removed by heat-induced aggregation and application of a magnetic field.¹¹ Additionally, the introduction of self-quenching

Received: June 19, 2015

Accepted: August 13, 2015

Published: August 13, 2015

fluorophores in thermoresponsive shells has been suggested and demonstrated as a way to determine the local temperature of magnetic particles in a biological environment or subject to alternating magnetic fields.^{18–20} Riffle and co-workers also showed that thermally induced aggregation of iron oxide nanoparticles greatly increases the T_2 contrast used for magnetic resonance imaging,¹⁹ which suggests dynamic and enhanced performance for biomedical imaging of nanoparticles that can undergo externally controlled aggregation. Using thermoresponsive, aggregating iron oxide nanoparticles it was also recently shown that the expulsion of water from close to the core above the LCST makes it possible to use such nanoparticles as nanoscopic thermometers to measure and image temperature change by magnetic resonance imaging.²¹

Encapsulation of iron oxide magnetic cores in thermoresponsive polymer shells has previously been attempted by a number of groups. Most research has focused on the formation of microgels or other large and disordered assemblies of thermoresponsive polymer and multiple magnetic cores.^{7,22–26} The coarse encapsulation in such systems leads to large particles with multiple cores and high polydispersity. Structurally more well-defined and smaller responsive nanoparticles would be beneficial when molecular-scale applications are approached and the bottom-up assembly of smart, responsive materials based on nanoparticle building blocks is desired. In several cases, the cores have been encapsulated by block copolymers,^{8,11,24,27,28} where one of the blocks is thermoresponsive (typically PNIPAM). In most cases, a core–shell structure has not been shown, which can be attributed to the common use of electrostatic, hydrophobic, or other weak multivalent anchoring of initiator or polymer to the cores.^{8,27,28} Transmission electron microscopy (TEM) inspection often show morphologies indicative of multiple core aggregates. The predominance of such aggregates was corroborated by hydrodynamic diameters far exceeding 100 nm, which is incompatible with individually stabilized core–shell architectures.^{23,24}

It is advantageous for all applications to have as well-defined nanostructures as possible, and for responsive nanoparticles this means that core–shell structures are typically preferred.⁶ A well-defined core–shell nanoparticle has individually stabilized spherical cores of low polydispersity, coated with a densely grafted polymer brush shell of defined thickness.¹ A controlled and monodisperse architecture ensures uniform properties that can be optimized for the application. We have therefore studied different approaches to graft PNIPAM brush shells onto monodisperse superparamagnetic iron oxide nanoparticles.

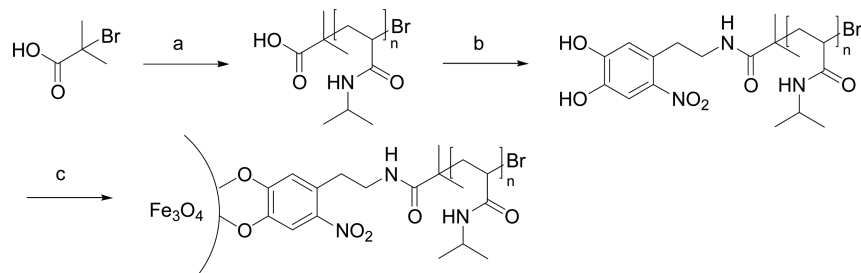
The common ways to functionalize nanoparticles with individual polymer dispersant shells and achieve a core–shell structure can be divided into “grafting-from” and “grafting-to” polymer grafting approaches. The grafting density that can be achieved is an important criterion to ensure the colloidal stability of core–shell nanoparticles. For superparamagnetic iron oxide nanoparticles, grafting densities of >0.5 chains/nm² of PEG-dispersants in the 3–10 kDa range have been reported necessary for colloidal stability;^{1,29} for reversibly thermally actuated nanoparticles the required grafting density might even be higher.

Grafting-to²⁶ and grafting-from^{25,27,30–35} for the preparation of metal/metal oxide–PNIPAM core–shell nanoparticles was performed on different cores (gold,^{32,36,37} silicon oxide,³⁵ iron oxide,^{25,26,30,38} zinc oxide³³) and with different polymerization methods (atom transfer radical polymerization

(ATRP),^{32,34,35,39} nitroxide mediated polymerization (NMP),³⁰ and reversible addition–fragmentation transfer radical polymerization (RAFT)).^{38,40} Quite often, the generated core–shell materials are analyzed via TGA, but no statement about the surface coverage is made.^{25,26,30,31,33,34} Only a few papers reported on the grafting density of PNIPAM by grafting-from approaches with values of 0.3 chains/nm² on iron oxide,³⁸ 0.45 chains/nm² on silicon oxide,³⁵ and 0.9 chains/nm² on gold.³² For grafting-to of PNIPAM, no literature value was found with respect to the grafting density but similar hydrophilic but not thermoresponsive polymers such as PEG have been studied. In particular, recent works have shown the challenge to achieve high grafting density with the grafting-to approach when the displacement of oleic acid from synthesis of monodisperse cores is required.^{29,41} We recently compared one-step and two-step grafting-to reactions of functionalized PEGs onto iron oxide nanoparticles.²⁹ Direct oleate ligand exchange with a nitrodopamine-PEG dispersant resulted in densities of ≤ 0.5 chains/nm², whereas modification of the surface with an amino-functionalized anchor and subsequent grafting of PEG under melt conditions led to grafting densities of 2–3 chains/nm² of PEG (5 kDa)²⁹ and an unusual star polymer-like shell density profile.⁴² For both grafting-from and grafting-to, the grafted polymer requires a chain termination binding to the inorganic nanoparticle core that replaces the oleic acid and forms a stable covalent bond.

An important aspect is that anchoring of the thermoresponsive dispersant should be through a linker that binds irreversibly and can withstand actuation at temperatures much higher than room temperature.^{1,4} The low average and with time decreasing grafting density resulting from using the strongly binding but reversible anchor dopamine⁴³ to anchor pH- and thermoresponsive shells to magnetic nanoparticles has been described by Schmalz and co-workers;³⁹ this results in increasing aggregation and increasingly difficult redispersion of nanoparticles under induced aggregation. Nitrocatechols represent a class of ligands that gives irreversible binding of a grafted polymer to iron oxide and that also withstands heating and other severe challenges.^{4,15,29,43} For thermally and especially magnetically actuated core–shell nanoparticles, this stability to heating is particularly important due to the high local temperatures expected from magnetic heating and the stress induced by strong deformation of the polymer shells. Therefore, our polymer dispersants and initiators were modified with nitrodopamine to serve as anchors to the nanoparticle surface.

In the few previous studies where PNIPAM-coated magnetic particles have been described, the spontaneous redispersion upon cooling of thermally aggregated particle suspensions is not discussed or redispersion is referred to as possible after sonication.¹⁹ This indicates that the grafting density or dispersant stability of all particles were not sufficient to keep the cores separated after aggregation; strong van der Waals attraction between cores at close proximity prohibits easy redispersion. The different grafting methods investigated in this work were therefore evaluated on their ability to produce individually dispersed NPs in water and the possibility to thermally and magnetically, completely and reversibly actuate aggregation of the NPs. The results suggest that densely grafted linear polymers of sufficiently high molecular weight are a necessary requirement to ensure spontaneous reversible aggregation and deaggregation of PNIPAM coated core–shell nanoparticles.

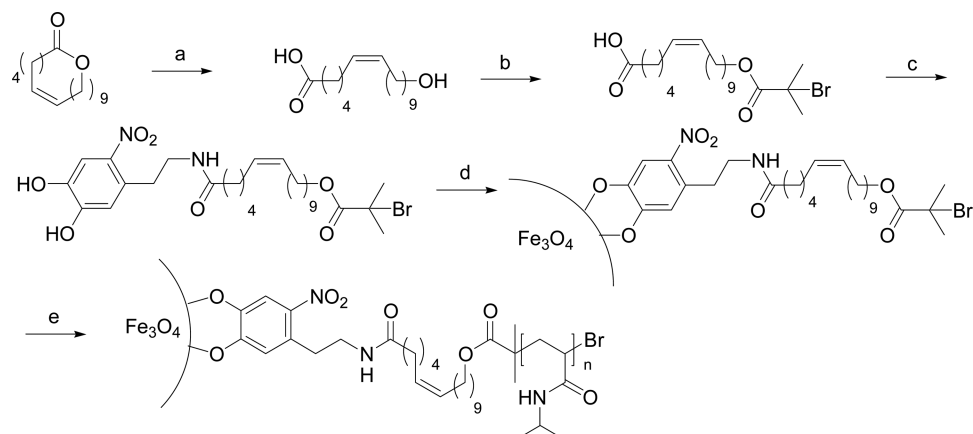
Scheme 1. Synthesis of Nitrocatechol Functionalized PNIPAM^a

^a(a) ATRP of NIPAM with acid functionalized initiator (water/methanol 9/1), CuBr, CuBr₂, tris[2-(dimethylamino)ethyl]amine (Me₆Tren), (b) 6-nitrodopamine hydrogensulfate, COMU, DMF, N,N-diisopropylethylamine, (c) grafting onto iron oxide nanoparticles, DMF, ultrasonication.

Table 1. PNIPAM Iron Oxide Core–Shell Nanoparticles by Grafting-to and Grafting-from

core diameter (nm) ^a	M_n PNIPAM-NDA (kDa) ^b	polydispersity D^c	weight loss (200–600 °C) (wt %) ^c	inorganic fraction ^c (wt %)	grafting density σ (chains/nm ²) ^c
3.9 ± 0.3 ^d	10	1.1	72	25	0.6
10.7 ± 0.9 ^d	20	1.2	74	21	1.0
5.6 ± 0.5 ^e	70	1.5	91	5	0.8

^aCore diameter determined by Pebbles⁴⁵ analysis of TEM images (≥ 100 particles). ^bMolecular weight determination by GPC in DMF (5 wt % LiBr), a correction factor ~2.7 was estimated from comparing GPC Polystyrene (PS) equivalent mass of an acid terminated PNIPAM (target MW 10 000 g/mol) with M_n determined by MALDI-TOF MS (see the Supporting Information, Figure S8). ^cWeight loss (200–600 °C) and inorganic fraction determined by TGA and grafting density calculated from average molecular weight, weight loss (200–600 °C), inorganic fraction and average core diameter (see the Supporting Information for example calculation), 100 wt % is the sum of weight loss 200–600 °C, inorganic fraction and mass loss from 25 to 200 °C (solvent traces, humidity). ^dParticles functionalized by grafting-to. ^eParticles functionalized by grafting-from.

Scheme 2. Synthesis of Surface Binding Initiator 4 and “Grafting-from” Polymerization of N-Isopropylacrylamide^a

^a(a) KOH, (b) 2-methyl-2-bromopropionyl bromide, triethylamine, (c) N-hydroxysuccinimide, 6-nitrodopamine hydrogensulfate, triethylamine, (d) ligand exchange reaction, (e) SI-ATRP of N-isopropylacrylamide.

RESULTS AND DISCUSSION

Core Synthesis. The oleic acid functionalized iron oxide nanoparticles were prepared with an adapted protocol described by Hyeon et al.⁴⁴ using thermal decomposition of iron pentacarbonyl in diethyl ether and oleic acid for stabilization and size regulation. The superparamagnetic magnetite nanoparticles are monocrystalline and display high sphericity and narrow size distributions as judged from transmission electron microscopy. Size determination was done using the freeware Pebbles⁴⁵ giving nanoparticle size distributions of 3.9 ± 0.3 nm and 10.7 ± 0.9 nm for the cores used for grafting-to modification and 5.6 ± 0.5 nm for the cores used for the grafting-from polymerization. After synthesis, the iron oxide cores are covered by a nonpolar shell of strongly

bound oleic acid, which has to be replaced with the PNIPAM dispersant or a surface binding initiator.

Polymer Shell Synthesis and Grafting. For the grafting-to approach, acid terminated poly(N-isopropylacrylamide) was prepared by ATRP using 2-methyl-2-bromopropionic acid as the initiator (Scheme 1). Polymers in the molecular weight range of 5 to 20 kDa could be prepared with low polydispersity (1.1–1.2). These precursor polymers were modified with 6-nitrodopamine using COMU as coupling agent (Scheme 1). Excess of the low molecular weight catechol was removed by dialysis, as it would compete with the polymer dispersant for binding sites on the nanoparticle surface.

The nitrodopamine-modified polymers were then reacted with oleic acid-capped iron oxide nanoparticles of different sizes (Table 1, Scheme 1) to graft PNIPAM chains onto the

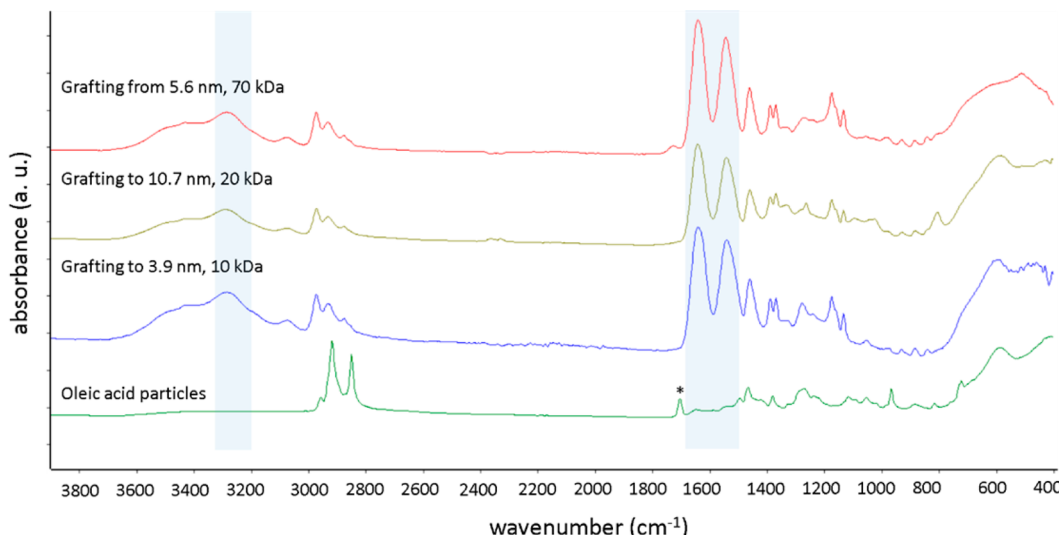


Figure 1. ATR-FTIR measurements for oleic acid coated iron oxide nanoparticles and PNIPAM functionalized nanoparticles synthesized with both the grafting-to and grafting-from methods. Characteristic peak for free or physisorbed oleic acid (marked by *) is absent for the PNIPAM-iron oxide core–shell particles. Characteristic bands at 3280, 1640, and 1540 cm^{-1} marked with light blue shadow can be assigned to the NH protons and the amide bond of the grafted PNIPAM.

nano particle surface. An excess of polymer, most often equivalent to 3 polymer chains/ nm^2 (iron oxide surface), was chosen to facilitate the ligand exchange. DMF was chosen as solvent for the ligand exchange, because it allows dissolution of both PNIPAM and oleic acid. The reaction was conducted under ultrasonication to disperse the nanoparticle cores in the reaction medium. Higher MW PNIPAM was chosen for the large core particles than for the small core particles to increase the shell thickness and thereby reduce potential interparticle interactions. After precipitation, the nanoparticles were purified by dialysis to remove excess dispersant and other reaction byproducts.

We additionally investigated the grafting-from approach. For the surface-initiated polymerization, initiator 4 was prepared in a three-step process, starting with base catalyzed hydrolysis of ω -6-hexadecenylactone (**Scheme 2**). Subsequently, the terminal hydroxyl group was esterified with 2-methyl-2-bromopropionyl bromide. The final step is the amidation with 6-nitro dopamine to generate initiator 4. Initiator particles were then prepared by ligand exchange of the oleic acid coated particles with initiator 4 in DMF. Analysis of the initiator particles (size $5.6 \pm 0.5 \text{ nm}$) by thermogravimetric analysis (TGA) gave a weight loss in the interval 200–600 °C of 59 wt % and an inorganic fraction of 37.7 wt %; this translates into a grafting density of 7.6 molecules/ nm^2 of initiator 4 on the iron oxide surface (assuming only initiator 4 in the shell). IR spectroscopy of these particles revealed a new band at 1725 cm^{-1} , which was assigned to the carbonyl group of the bromoisobutyrate. Free and bound remaining oleic acid were still detected (for a detailed IR-analysis, see the **Supporting Information**, Figure S7). This explains the overestimate of the grafting density of the initiator (higher than the theoretical highest grafting density), which was caused by the additional oleic acid mass in the sample.

The particles were then used for the surface-initiated ATRP of N-isopropylacrylamide (NIPAM). From literature, it is known that the ATRP of NIPAM proceeds in a living fashion in the presence of water.^{46,47} The hydrophobic initiator particles were not soluble in water or water/methanol mixtures and thus

had to be dispersed through sonication. In the course of the polymerization, the nanoparticles become soluble in the reaction solvent, due to growth of the hydrophilic shell. Coarse purification of the nanoparticles was done by dissolving the crude product in tetrahydrofuran (THF), precipitation in diethyl ether and subsequent magnetic decantation. Residual free polymer was removed by dialysis in water using membranes with a cutoff size of 1000 kDa to take into account the large coil size of PNIPAM in water. The high molecular weight cutoff corresponds to a pore size $>30 \text{ nm}$, which ensures that the PNIPAM in hydrated coil conformation can pass through the pores while nanoparticles were retained. To verify that all free PNIPAM was removed, dialysis for an additional day was performed, which resulted in no further reduction of organic content measured by TGA. For molecular weight determination, the shell polymer was cleaved off by treating the core–shell nanoparticles with diluted hydrochloric acid (1 M). GPC analysis of the cleaved off polymer gave a molecular weight of 70 kDa and a polydispersity of 1.5, which is in the range of controlled radical polymerization.

Characterization of the Polymer Shell. **Figure 1** shows attenuated total reflection-Fourier transform infrared spectroscopy (ATR-FTIR) measurements of the grafting-to and grafting-from samples. The spectra of the grafting-to samples confirm successful ligand exchange from oleic acid to catechol-modified PNIPAM, with new bands at 3280, 1640, and 1540 cm^{-1} that can be assigned to the NH protons and the amide bond of the grafted polymer.⁴⁸ The broad band in the range of 400 to 600 cm^{-1} can be assigned to the presence of the iron oxide core. The spectrum of the grafting-from sample resembles the grafting-to products, which demonstrates successful polymerization of PNIPAM shells on the cores. A small sideband at 1725 cm^{-1} is attributed to the ester bond of the surface bound initiator. The presence of bound oleic acid cannot be excluded by evaluating characteristic bands in the range from 1420 to 1550 cm^{-1} , because the polymer bands dominate the spectrum in this region. However, a characteristic peak of free or physisorbed oleic acid^{49,50} at 1702 cm^{-1} was not present in the final product. The difficulty of totally replacing

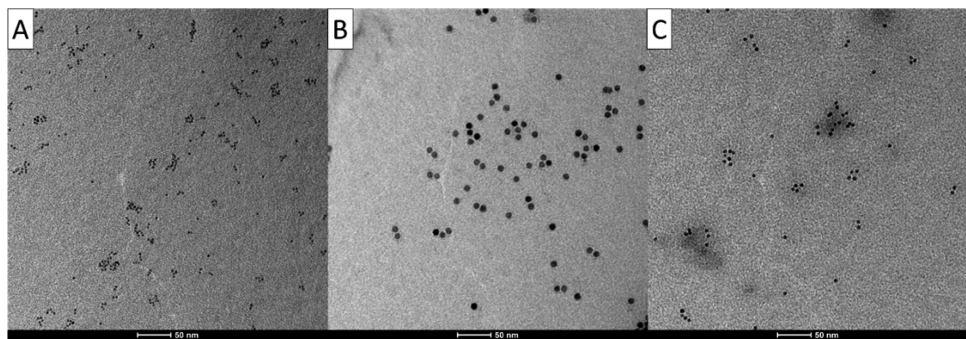


Figure 2. TEM images of iron oxide–PNIPAM core–shell nanoparticles formed by ligand exchange grafting-to synthesis, (A) core, 3.9 nm, PNIPAM 10 kDa; (B) core 10.7 nm, PNIPAM 20 kDa; or grafting-from polymerization (C) core 5.6 nm, PNIPAM 70 kDa.

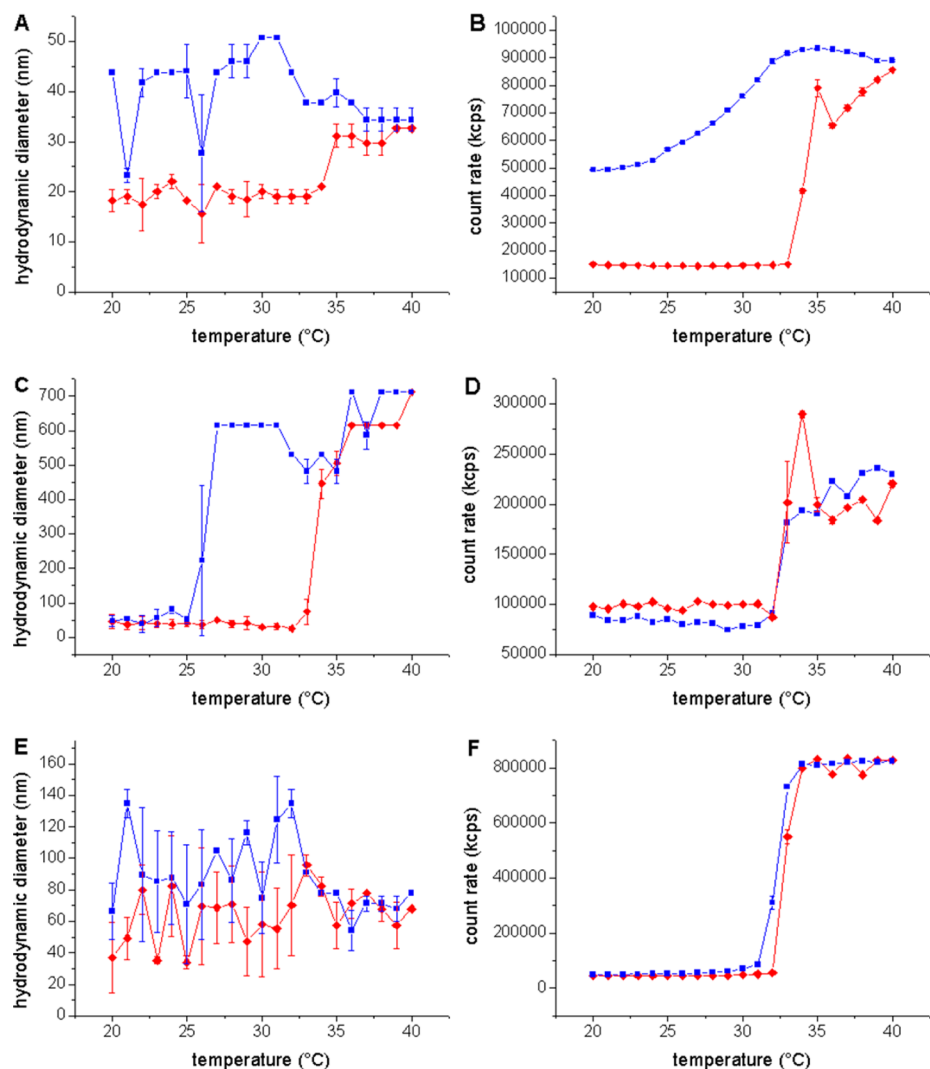


Figure 3. Dynamic light scattering data showing hydrodynamic diameter (main peak of the number weighted size distribution) and intensity count rate vs temperature. Heating (red diamonds) and cooling steps (blue squares) were 1 °C with 5 min to equilibrate at each measurement point, symbols represent mean values from 3 runs with error bars giving the standard deviation, (A and B) grafting-to 3.9 nm core/PNIPAM 10 kDa, (C and D) grafting-to 10.7 nm core/PNIPAM 20 kDa, (E and F) grafting-from 5.6 nm core/PNIPAM 70 kDa.

oleic acid even with a more strongly binding dispersant was recently demonstrated.⁴¹

TGA was performed in synthetic air (to combust completely all organic material⁵¹) to estimate the total organic content (TOC) of the nanoparticle sample corresponding to the amount of grafted polymer. The total organic content was

calculated from the weight loss from 200 to 600 °C. Below 200 °C, mass loss is mainly due to evaporation of solvent and the combustion of the shell is completed at 600 °C. The mass loss curves exhibit a two-step profile (see the Supporting Information, Figure S3). The average grafting density of PNIPAM can be calculated by dividing the weight loss (200–

600 °C) by the total surface area of the particles (calculated from the particle size and the inorganic weight fraction) and by assuming the average molecular weight of the PNIPAM dispersant. A grafting density of ~0.6 chains/nm² was calculated from TGA for the grafting-to particles with 3.9 nm cores and ~1.0 chains/nm² for the grafting-to particles with 10.7 nm cores (see Table 1). Such grafting densities have previously been discussed as a threshold for colloidal stability of superparamagnetic nanoparticles in complex media and under thermal actuation.^{1,29,43} The relatively high grafting density for the grafting-to approach when compared to planar surfaces and previous reports, can be explained by the care taken to minimize the coil size of the PNIPAM-nitrodopamine during ligand replacement. The coil size footprint determines the grafting density if sufficiently high affinity can be achieved for the polymer anchor group under conditions that solubilize the oleic acid covering the core surface.²⁹ On a highly curved nanoparticle surface the effective highest achievable grafting density will be higher than on a planar surface has more severe steric constraints.¹

The grafting-from particles with 5.6 nm cores had a grafting density of ~0.8 chains/nm². The relatively low density of the surface initiated polymerization can be attributed to low surface coverage of initiator. IR analysis of the initiator particles showed residual free and bound oleic acid (see the Supporting Information, Figure S7). Even if a minor, in the case of the grafting-to samples undetected, fraction of oleic acid could still be present on the surface as described above,⁵² this would not significantly affect the determination of the grafting density due to the much higher molecular weight of the grafted PNIPAM than of oleic acid. In summary, all achieved grafting densities are sufficient to achieve colloidal stability at physiological temperatures when compared to literature.¹ The grafting density achieved for the large core particles by grafting-to and by grafting-from should also be sufficient for smart materials applications where cores might aggregate and have to redisperse.^{6,43,53} However, in none of the cases was a grafting density achieved that is expected to go beyond a spherical brush to a star polymer-like density profile as was recently reported for core–shell particles.^{42,54}

The PNIPAM-grafted core–shell nanoparticles were inspected by TEM and showed highly monodisperse, individually separated nanoparticles dried on the grid, with no change to core morphology (Figure 2). For particles produced by grafting-from, some clusters of cores could be observed on the grid (see the Supporting Information, Figure S9). Although the bulk aggregation state of nanoparticles cannot be directly determined after drying onto TEM grids, it is possible that the difficulty to disperse the initiator-coated cores in water mixtures at the start of the polymerization led to some growth proceeding from aggregated clusters of cores and that it is those aggregates that are observed on the TEM grid. The cores in such clusters would effectively share a common dense PNIPAM shell. The grafting-from samples had a much lighter color than the grafting-to samples; this is also indicative of a nonhomogenous distribution of cores at the same concentration. If clusters are indeed present, it means that the local grafting density for the exposed surface of the grafting-from particles presented in Table 1 should be adjusted slightly upward; however, it also results in an intrinsic higher polydispersity due to the fraction of clusters.

Thermally Induced Aggregation and Redispersion. The size and reversible aggregation of the individually stabilized

core–shell nanoparticles at a concentration of one mg/mL in ultrapure water were studied by dynamic light scattering (DLS) (Figure 3). The hydrodynamic sizes determined at room temperature (20 °C) by DLS were 19 nm for the 3.9 nm/10 kDa PNIPAM and 45 nm for the 10.7 nm core/20 kDa PNIPAM particles. The grafting-from particles had a hydrodynamic diameter of 30–40 nm, but possibly due to the presence of clustered cores some uncertainty in the determination of the hydrodynamic diameter was observed. The DLS detector count rate (Figure 3B,D,F) is a sensitive measure of aggregation due to its strong scaling with aggregate size, and it provides a less biased measure than the main number peak size determined by the built-in CONTIN algorithm (Figure 3A,C,E). However, the count rate recorded at a single angle in DLS is susceptible to the influence of many parameters of the sample, such as changes in size and refractive index that change the scattering angle distribution and thereby the count rate at a fixed detector angle. The interpretation of a change in count rate is therefore not unambiguous. Nonetheless, it provides a sensitive indicator to determine the temperature-induced onset of aggregation and deaggregation through a mere change in count rate.

Upon heating, a distinct increase in the count rate followed by an increase in the main peak size is observed at temperatures corresponding closely to the LCST of free PNIPAM in water (32 °C for 10.7 nm/20 kDa, 33 °C for 3.9 nm/10 kDa and 32 °C for the grafting-from particles). The small difference in observed LCST between the samples is not likely to be due to a real difference in LCST of the polymer due to differences in grafting, because the determination of the LCST is sensitive to the few data points acquired within the transition region. Although a clear increase in size and count rate was measured, visual inspection of the solutions (concentration: 1 mg/mL) above their respective LCST did not show any turbidity; this indicates a low level of weak aggregation and only small cluster size. Increasing the concentration to 5 mg/mL resulted in turbid samples and some reversible precipitation; this confirms the expectation of a concentration dependent aggregation and precipitation for weakly aggregating colloids.

Significant hysteresis was observed in DLS upon cooling. The hysteresis was more pronounced in the main hydrodynamic size peak than in the count rate. Indeed, the small nanoparticles spontaneously never fully recovered to the initial count rate and size values during the measurement. Although, the difference between the small and large nanoparticles could be related to size, we hypothesize that this incomplete recovery is related to the lower dispersant density and thinner shell grafted to the 3.9 nm/10 kDa nanoparticles. A thinner polymer shell leads to closer proximity of the cores during aggregation and therefore stronger particle–particle adhesion that has to be overcome when the PNIPAM rehydrates below the LCST. Additional energy input through mild agitation redispersed also these nanoparticles at room temperature.

Our results show the LCST to be independent of grafting method and grafting density within the investigated interval of grafting densities. Such independence has been observed for planar PNIPAM brushes at lower grafting density than on our nanoparticles but for similar PNIPAM molecular weight. However, recent reports^{55,56} have described large increases in the LCST of PNIPAM hydro- and microgels with increasing concentration of incorporated iron oxide nanoparticles. In view of our results, it is likely that the increase in LCST in these studies is related to the increasing direct interaction of

PNIPAM chain segments with the unfunctionalized iron oxide nanoparticle surfaces as the nanoparticle concentration is increased. In our core–shell nanoparticle system, the PNIPAM chains are densely end-grafted through the nitrodopamine anchor, which limits the access of free chain segments to the iron oxide surface, and neither dependence on grafting density nor on particle concentration is observed for the LCST. Further support for this interpretation is lent by previous findings for PNIPAM adsorbed to silica, showing a loss of responsiveness when directly adsorbed to colloid surfaces at low density and recovered responsiveness at higher surface densities that force extension of more polymer segments away from the particle surface.⁵⁷

The aggregate hydrodynamic size measured by DLS stayed at almost the same value at temperatures above the LCST. This behavior was previously observed for individually stabilized (small; 4 nm and polydisperse) thermoresponsive nanoparticles,²³ and was then suggested to indicate the ability to tailor cluster size by nanoparticle properties. It can be observed that the small (3.9 nm core/10 kDa) nanoparticles produced clusters with negligibly larger sizes than the individual particles, indicative of only a few cores per aggregate. However, the large (10.7 nm core/PNIPAM 20 kDa) nanoparticles produced aggregates that were 1 order of magnitude larger than the individual nanoparticles; large aggregate size will facilitate magnetic separation. Thanks to the dense and thick shell (high grafting density and high PNIPAM dispersant molecular weight) of the 10.7 nm core/PNIPAM 20 kDa, these particles also showed spontaneous redispersion upon cooling as monitored by the scattering intensity, which is additionally beneficial for magnetic separation applications.

The grafting-from particles also have a dense and thick PNIPAM shell. These particles also displayed spontaneous and complete redispersion upon cooling as monitored by the scattering intensity. The hydrodynamic diameter measured for these samples was too variable to make any conclusions about size changes and thermally aggregated cluster sizes. The scattering intensity increases strongly with size, although other factors such as changes in refractive index and precipitation also have a strong influence; it is likely that the hypothesized clustered cores in a fraction of the sample strongly influence the determination of the main number weighted peak size plotted in Figure 3. Summing up, combined with the result for the large grafting-to cores, this result supports the conclusion that a dense and thick spherical brush end-grafted to the inorganic core is key to full, spontaneous, and reversible thermal actuation.

Interestingly, in early studies on PNIPAM encapsulating multiple magnetic cores or on large PNIPAM-gel particles coated with magnetic particles the hydrodynamic diameter was measured to decrease with increased temperature.^{23–25} The relative decrease in size in these studies was always minor compared to the known volume change of PNIPAM above the LCST. This might again be due to the uncontrolled direct interaction of polymer with the nanoparticle surface for such colloids leading to a loss of responsiveness.⁵⁷ Thus, the small relative volume change and the reduction instead of increase in size point to weak desolvation and lack of aggregation; this would be disadvantageous to applications relying on particle extraction as will be demonstrated below. The individually stabilized thermoresponsive core–shell nanoparticles presented in our work display a more desirable behavior in this respect.

Thermally Induced Aggregation and Magnetic Extraction. Well-stabilized core–shell superparamagnetic nanoparticles cannot be aggregated and extracted by the field of even a strong permanent magnet or magnetic column. However, if the hydration of the shell is reduced and weak aggregation of the nanoparticles occurs, the aggregates can be extracted by much lower magnetic field gradients. The low LCST of PNIPAM makes this transition possible at temperatures that are compatible with handling biomolecules. PNIPAM-grafted superparamagnetic particles could therefore be of interest to enhance performance of magnetic extraction columns for fishing, e.g., proteins out of complex biological fluids.

Figure 4A shows the stability of the 10.7 nm core/20 kDa PNIPAM superparamagnetic particles to the magnetic field

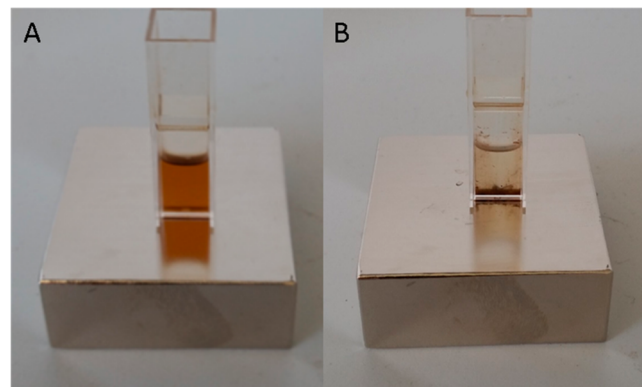


Figure 4. Sample (10.7 nm/PNIPAM 20 kDa, 5 mg/mL) in a poly(methyl methacrylate) (PMMA) cuvette placed upon a neodymium magnet, (A) at room temperature, (B) at 40 °C. In plastic cuvettes, a discoloration of the cuvette wall remains, interpreted as a high affinity of the dehydrated PNIPAM for the cuvette walls.

produced by a strong permanent magnet at room temperature below the LCST; all the individually stabilized particles remain dispersed. Upon heating to 40 °C (above the LCST of 32 °C), the core–shell particles weakly aggregate as shown by the DLS measurements above. The aggregates in the turbid particle dispersion can then be attracted by the same magnetic field (Figure 4B). The almost complete extraction of nanoparticles observed at moderate heating with a standard magnet contrasts to the incomplete withdrawal demonstrated earlier by nanoparticles with a physisorbed block copolymer PNIPAM shell architecture¹¹ or by polydisperse PNIPAM-grafted nanoparticles.¹⁹ Upon cooling below the LCST, the brown precipitate was redissolved by gentle shaking, demonstrating the reversibility of the process and the stability of the core–shell nanoparticles against thermal stress.

Magnetic Heating. Superparamagnetic nanoparticles interact with an externally applied oscillating magnetic field of the right frequency to produce heat by Néel relaxation.⁴ Large ferromagnetic particles coated by random block copolymer with PNIPAM blocks have been shown to not pass a size exclusion column during the application of an alternating magnetic field that raised the bulk temperature of the solution above the LCST.⁵⁸ It is conceivable that desolvation of the shell leading to aggregation of the nanoparticles could be achieved exclusively through the application of an alternating magnetic field, because the heat produced by magnetic heating is locally produced in the center of the PNIPAM polymer brush grafted to the nanoparticle core surface. That magnetic heating changes

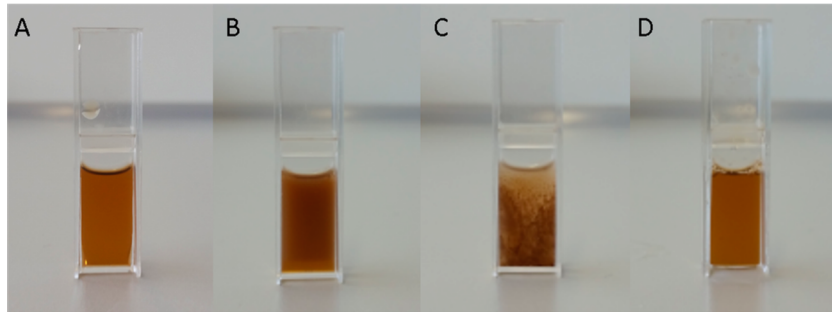


Figure 5. Magnetic actuation of iron oxide PNIPAM nanoparticles (grafting-to, core 10.7 nm/PNIPAM 20 kDa), dissolved in water (5 mg/mL), (A) clear dispersion before magnetic actuation, solution temperature 24 °C, (B) aggregation and turbidity after 5 min actuation, solution temperature 32.4 °C, (C) precipitation after 10 min actuation, solution temperature 35.7 °C, (D) redispersion of aggregated particles after cooling down to below the LCST.

the solvation of the shell without change in the bulk temperature above the LCST is suggested by results by Rinaldi and co-workers on iron oxide nanoparticles with a PNIPAM shell incorporating fluorophores.¹⁸ To investigate this hypothesis applied to magnetic separation, we exposed the largest nanoparticle (10.7 nm core/20 kDa PNIPAM) at a concentration of 5 mg/mL in water to a magnetic field at 228 kHz using an Ambrell magnetic heater. The largest cores are expected to lead to the most efficient magnetic heating response. After 5 min actuation, the initially clear brown solution (Figure 5A) turned turbid (Figure 5B). The bulk solution temperature at this point was 32.4 °C, which equals the LCST of the PNIPAM in the shell. A brown precipitate was visible after actuation for additionally 5 min (Figure 5C), at which point the bulk solution temperature had increased to 35.7 °C. After cooling down, the precipitate easily redispersed by gentle shaking (Figure 5D), proving the reversibility of the magnetic heating cycle just as for the purely thermally actuated particles. Analogous experiments with the same sample at a concentration of 1 mg/mL did not show turbidity or aggregation after prolonged magnetic actuation for 20 min (bulk solution temperature: 37.2 °C), although particle aggregation was clearly shown for purely thermal heating at this concentration by DLS.

Turbidity will be observed when particles with desolvated shells collide and aggregate to aggregates that on average are large enough to scatter light strongly. This transition should therefore depend on the concentration of the sample (controlling the frequency of collisions) and the degree of desolvation and collapse of the PNIPAM shell (controlling the probability to aggregate upon collision and the probability to desorb from an aggregate). The latter will depend on the local temperature, which is a balance of the heat produced by the magnetic core in the oscillating magnetic field and the heat transfer (diffusion) from the core to the bulk liquid.

Our result demonstrates that magnetic heating can be used to efficiently and reversibly aggregate PNIPAM-grafted superparamagnetic nanoparticles. However, at least at concentrations up to 5 mg/mL of large 10.7 nm core/PNIPAM 20 kDa superparamagnetic nanoparticles and with a standard magnetic heater without optimization, the difference in the rates of heat generation and heat diffusion is not large enough to dehydrate the entire shell and thereby cause sufficient particle–particle affinity to cause aggregation upon nanoparticle collision; this only occurs after the magnetic heating has led to a global rise in temperature. Heat diffusion in water is fast and apparently sufficiently efficient for the outer part of the shell of suspended

nanoparticles to still be highly solvated and serve to prevent the core–shell nanoparticles from aggregating. The heat generation in our quite concentrated nanoparticle system was, however, sufficiently efficient to heat the entire bulk solution to the LCST within 5 min, at which point aggregation was observed; strong aggregation and precipitation was observed after 10 min of magnetic heating.

It is important to note that precipitation was not the result of nanoparticle destruction; the nanoparticles could easily be redispersed after cooling. This stability can only be observed when an anchor chemistry like nitrodopamine is used that can withstand the high local temperature that is produced by the Néel relaxation heating of the magnetic core.

For the grafting-from sample, the same experiment was conducted (see the Supporting Information, Figure S1). The time until the solution turned turbid was longer (8 min) in accordance with the lower volume fraction of iron oxide. The bulk solution temperature was again 32 °C when the onset of turbidity was observed. Additional actuation for 10 min, which increased the bulk temperature to 36 °C, did not lead to stronger aggregation and precipitation. Also, this sample redissolved spontaneously upon cooling. The difference in the strength of aggregation between the grafting-from and grafting-to samples could be explained by the thicker shell (higher PNIPAM molecular weight) of the grafting-from samples. This would facilitate the separation of the core–shell structures and also possibly lead to higher interparticle repulsion in the outer parts of the shell, especially during magnetic heating. Testing of more comprehensively varied samples to also rule out any particle concentration effects would be required to verify such an effect.

CONCLUSIONS

We have demonstrated that colloidally stable superparamagnetic iron oxide core nanoparticles with densely grafted PNIPAM shells can be obtained by both grafting-to and grafting-from methods to form the thermoresponsive polymer brush shell. Grafting-to and grafting-from yielded similar grafting densities. The lower than expected grafting density obtained by grafting-from highlighted the difficulty to replace oleic acid by an active hydrophobic initiator efficiently. The achieved grafting density is still in the upper range of grafting densities reported for metal/metal oxide–PNIPAM core–shell nanoparticles. Additionally, dispersion of initiator-coated particles under conditions where efficient polymerization could be performed was challenging, and seemed to result in small, but stable, clusters forming within a single shell. Still,

grafting-from allowed us to reach high molecular weights of the brush polymer, translating into higher brush thickness, which would be unlikely to achieve by grafting-to in a direct ligand exchange reaction where the polymer coil size during ligand replacement determines the maximum achievable grafting density.

High grafting density and molecular weights ≥ 20 kDa PNIPAM were observed necessary for fully reversible thermal or magneto-thermal aggregation of nanoparticles with rapid redispersion upon cooling. Sufficient grafting densities of > 0.5 chains/nm² for this molecular weight could be reached also by the grafting-to method. The key to this achievement is the use of the high-affinity single anchor group nitrodopamine and grafting during conditions of low coil size. The use of end-grafted PNIPAM brushes resulted in retained LCST independent of grafting density. These achievements opened exciting opportunities to explore thermal heating combined with magnetic extraction and redispersion as well as aggregation and redispersion controlled exclusively by magnetic heating through an externally applied alternating magnetic field. These possibilities were demonstrated with aggregation being possible within minutes at relevant concentrations using magnetic heating. The thermally stable anchoring of the PNIPAM dispersant through nitrodopamine to the iron oxide nanoparticle surface ensured that the process could be reversibly repeated without observable deterioration in particle properties.

Interesting next steps would be, e.g., the addition of binding sites to the PNIPAM shell that would allow for controlled capture, magneto-thermal aggregation, extraction and release of specifically bound biomolecules in integrated systems, as well as enhanced targeted magnetic resonance imaging and therapy utilizing the stronger response of induced particle aggregates.

EXPERIMENTAL SECTION

Materials. All chemical were purchased from Sigma-Aldrich and were used without further purification except *N*-isopropylacrylamide (NIPAM), which was recrystallized from hexane/toluene v/v: 1/1. Synthesis of oleic acid coated iron oxide nanoparticles is described in detail in Zirbs et al.²⁹

Synthesis of Acid Terminated PNIPAM (M_n 10 000 g/mol).

NIPAM (1 g, 8.8 mmol), CuBr (13 mg, 0.09 mmol), CuBr₂ (2 mg, 0.009 mmol), and 2-methyl-2-bromopropionic acid (16.7 mg, 0.1 mmol) were weighed in a flask, and 9 mL of Milli-Q water and 1 mL of methanol were added. The flask was closed with a septum and the solution was purged for 20 min with nitrogen. The solution was cooled in an ice bath. Tris[2-(dimethylamino)ethyl]amine (Me₂Tren) (40 μ L, 0.15 mmol) was dissolved in Milli-Q water (1 mL), and the solution was purged with nitrogen for 20 min. The ligand solution was injected to the monomer solution to start the polymerization. After 24 h, the flask was opened to air. The polymer was isolated by heating the solution to 50 °C. The supernatant was disposed. After drying, the crude product was dissolved in THF and precipitated in cold diethyl ether. The polymer was collected via centrifugation and dried in a desiccator. Yield: 980 mg (98%).

Synthesis of NDA Terminated PNIPAM (M_n 20 000 g/mol).

Acid-terminated PNIPAM (2 g, 0.1 mmol), COMU (51 mg, 0.12 mmol) and DIPEA (17 μ L, 0.1 mmol) were weighed in a flask. The mixture was dissolved in DMF (20 mL), purged with nitrogen for 5 min, and stirred for 1 h, during which the solution turned yellow. 6-Nitrodopamine hydrogensulfate (89 mg, 0.3 mmol) in DMF (1 mL) and DIPEA (34 μ L, 0.2 mmol) were added, and the resulting solution was stirred at room temperature for 3 days. The solution was acidified with a few drops of 2 M HCl. The polymer was precipitated by dropping the solution in cold diethyl ether, collected via centrifugation, dissolved in water and dialyzed against distilled water until the water remained clear (membrane cutoff size 3.5 kDa). The

NDA terminated polymer was obtained after freeze-drying in a yield of 1.4 g (70%). ¹H NMR (300 MHz, CD₃OD, δ): 7.56 (s, 1H), 6.71 (s, 1H), 3.97 (s, 1H, PNIPAM), 3.48 (m, 2H), 3.05 (t, 2H), 0.91–2.36 (m, 9H, PNIPAM), functionality (60–70%).

"Grafting-to" for the Preparation of Iron Oxide – PNIPAM Core–Shell Nanoparticle. As synthesized oleic acid capped nanoparticles (300 mg, inorganic fraction, 30 wt %; core diameter, 10.7 nm) and NDA terminated PNIPAM (1.4 g, M_n : 20 000 g/mol) were suspended/dissolved in DMF (20 mL). The solution was purged for 10 min with nitrogen and then sonicated for 24 h. Subsequently, the core–shell NPs were precipitated in diethyl ether, washed with *n*-hexane and air-dried. The crude product was dissolved in Milli-Q water and dialyzed against distilled water for 24 h (membrane cutoff size 1000 kDa). The resulting solution was filtered and freeze-dried to obtain PNIPAM-grafted iron oxide nanoparticles (200 mg).

"Grafting-from" Polymerization. NIPAM (1 g, 8.80 mmol) and PMDETA (55 μ L, 0.26 mmol) were dissolved into a mixture of water (3.13 mL) and methanol (0.35 mL). The solution was purged with nitrogen for 15 min and then added to a nitrogen-purged flask containing copper(I) bromide (13 mg, 0.09 mmol) and copper(II) bromide (2 mg, 0.009 mmol). After stirring for 30 min, the solution was transferred to a nitrogen-purged flask containing initiator particles (for synthesis, see the Supporting Information) (35 mg) suspended in methanol (1 mL) and stirred at maximum speed. The polymerization was quenched after 20 h by opening the reaction flask to air. The core–shell particles were isolated by heating the solution to 50 °C, dried, dissolved in THF and precipitated into cold diethyl ether. The precipitate was coarsely purified by magnetic decantation. The black, rubber-like material was dried, dissolved in water, and dialyzed for 24 h against Milli-Q water (membrane cut off size: 1000 kDa). Yield: 290 mg.

Analytics. **TEM.** Transmission electron micrographs were recorded on a FEI Tecnai G2, with 160 kV acceleration voltage on silicon monoxide coated grids. Nanoparticle size distributions were calculated with the freeware Pebbles based on the analysis of ≥ 100 particles.⁴⁵

ATR-FTIR. IR spectra were recorded on a Bruker Tensor 37 FTIR spectrometer.

DLS. Hydrodynamic size, LCST, and temperature cycling experiments were conducted on a Malvern Zetasizer Nano-ZS. Mean values and standard deviation were calculated from 3 runs. Samples were dissolved in Milli-Q water at a concentration of 1 mg/mL and filtered with a RC filter 0.45 μ m. This concentration was chosen due to the absence of visible precipitation while yielding observable temperature-dependent aggregation.

TGA. Thermal gravimetric analysis was performed on a Mettler Toledo TGA/DSC1, with 80 mL/min synthetic air as reactive gas and 20 mL/min nitrogen as protective gas and a heating rate 10 K/min from 25 to 600 °C.

NMR. ¹H- and ¹³C NMR were measured on a BRUKER AV III 300 spectrometer. Chemical shifts were recorded in ppm and referenced to residual protonated solvent (CDCl₃: 7.26 ppm (¹H), 77.0 ppm (¹³C)). DMSO-*d*₆: 2.50 ppm (¹H), 39.4 ppm (¹³C). D₂O: 4.79 ppm (¹H)).

MALDI-TOF MS. MALDI mass spectra were measured on a Bruker Autoflex speed. Matrix (dithranol in THF (20 mg/mL)) was mixed with the sample and dropped on the sample holder. No salt was added.

GPC. For GPC measurements, an adapted Dionex HPLC was utilized with a P680 HPLC pump, an ASI-100 autosampler and a STH585 column oven. The GPC setup consists of three MZ Gel SDPlus columns (a precolumn followed by two columns with separation ranges of 10–2000 and 1–40 kDa, respectively). As a detector, a Knauer Smartline RI Detector 2300 was applied. As eluent, DMF with 5 wt % LiBr was used. Samples with a concentration of 3 mg/mL were injected and measured at 60 °C with a flow rate of 0.8 mL/min. As software Chromeleon 6.80 with the extension pack V02 was used. Polystyrene standards 1.5–651 kg/mol were used for external calibration.

Magnetic Actuation. Magnetic heating of the nanoparticles was performed with an Ambrell Easy Heat LI, with a current of 438.9 A and a frequency of 228 kHz, coil dimension (height \times outer diameter \times coil thickness \times number of turns = 37 mm \times 37 mm \times 2 mm \times 6).

The sample was dissolved in Milli-Q water at a concentration of 5 mg/mL and filtered with a RC filter 0.45 μm.

ASSOCIATED CONTENT

Supporting Information

The Supporting Information is available free of charge on the ACS Publications website at DOI: [10.1021/acsami.5b05459](https://doi.org/10.1021/acsami.5b05459).

Preparation of initiator 4 and initiator particles, FTIR analysis of initiator particles, magnetic actuation and magnetic extraction of grafting from sample, TGA curves and analysis, MALDI-TOF MS of PNIPAM ([PDF](#)).

AUTHOR INFORMATION

Corresponding Author

*E. Reimhult. E-mail: erik.reimhult@boku.ac.at. Phone: +43-1-47654-2230. Fax: +43-1-47891-12.

Notes

The authors declare no competing financial interest.

ACKNOWLEDGMENTS

The research leading to these results was funded by the European Research Council under the European Union's Seventh Framework Program (FP/2007-2013)/ERC Grant Agreement no. 310034 and the Hochschuljubiläumsstiftung der Stadt Wien (H-2432/2012 and H-284635/2014). We thank Tanja Zwölfer and Behzad Shirmardi Shaghaseemi for support with the core and nitrodopamine synthesis. We thank Prof. Dieter Baurecht from the University of Vienna for access to ATR-FTIR spectroscopy and acknowledge the VIBT Extremophile Center for access to TGA.

REFERENCES

- (1) Amstad, E.; Textor, M.; Reimhult, E. Stabilization and Functionalization of Iron Oxide Nanoparticles for Biomedical Applications. *Nanoscale* **2011**, *3*, 2819–2843.
- (2) Veiseh, O.; Gunn, J. W.; Zhang, M. Q. Design and Fabrication of Magnetic Nanoparticles for Targeted Drug Delivery and Imaging. *Adv. Drug Delivery Rev.* **2010**, *62*, 284–304.
- (3) Xu, C. J.; Sun, S. H. Monodisperse Magnetic Nanoparticles for Biomedical Applications. *Polym. Int.* **2007**, *56*, 821–826.
- (4) Reimhult, E. Nanoparticle-Triggered Release from Lipid Membrane Vesicles. *New Biotechnol.* **2015**, *32*, 665–672.
- (5) Heskins, M.; Guillet, J. E. Solution Properties of Poly(N-Isopropylacrylamide). *J. Macromol. Sci., Chem.* **1968**, *2*, 1441–1455.
- (6) Motornov, M.; Roiter, Y.; Tokarev, I.; Minko, S. Stimuli-Responsive Nanoparticles, Nanogels and Capsules for Integrated Multifunctional Intelligent Systems. *Prog. Polym. Sci.* **2010**, *35*, 174–211.
- (7) Rubio-Retama, J.; Zafeiropoulos, N. E.; Serafinelli, C.; Rojas-Reyna, R.; Voit, B.; Cabarcos, E. L.; Stamm, M. Synthesis and Characterization of Thermosensitive Pnipam Microgels Covered with Superparamagnetic $\gamma\text{-Fe}_2\text{O}_3$ Nanoparticles. *Langmuir* **2007**, *23*, 10280–10285.
- (8) Wu, X.; He, X.; Zhong, L.; Lin, S.; Wang, D.; Zhu, X.; Yan, D. Water-Soluble Dendritic-Linear Triblock Copolymer-Modified Magnetic Nanoparticles: Preparation, Characterization and Drug Release Properties. *J. Mater. Chem.* **2011**, *21*, 13611–13620.
- (9) Hosta-Rigau, L.; Staedler, B.; Yan, Y.; Nice, E. C.; Heath, J. K.; Albericio, F.; Caruso, F. Capsosomes with Multilayered Subcompartments: Assembly and Loading with Hydrophobic Cargo. *Adv. Funct. Mater.* **2010**, *20*, 59–66.
- (10) Staedler, B.; Price, A. D.; Zelikin, A. N. A Critical Look at Multilayered Polymer Capsules in Biomedicine: Drug Carriers, Artificial Organelles, and Cell Mimics. *Adv. Funct. Mater.* **2011**, *21*, 14–28.
- (11) Zhao, Q.; Chen, N.; Zhao, D.; Lu, X. Thermoresponsive Magnetic Nanoparticles for Seawater Desalination. *ACS Appl. Mater. Interfaces* **2013**, *5*, 11453–11461.
- (12) Lai, J. J.; Hoffman, J. M.; Ebara, M.; Hoffman, A. S.; Estournes, C.; Wattiaux, A.; Stayton, P. S. Dual Magnetic-/Temperature-Responsive Nanoparticles for Microfluidic Separations and Assays. *Langmuir* **2007**, *23*, 7385–7391.
- (13) Chen, Y.; Bai, Y.; Chen, S.; Ju, J.; Li, Y.; Wang, T.; Wang, Q. Stimuli-Responsive Composite Particles as Solid-Stabilizers for Effective Oil Harvesting. *ACS Appl. Mater. Interfaces* **2014**, *6*, 13334–13338.
- (14) Gajda, A. M.; Ulbricht, M. Magnetic Fe_3O_4 Nanoparticle Heaters in Smart Porous Membrane Valves. *J. Mater. Chem. B* **2014**, *2*, 1317–1326.
- (15) Amstad, E.; Kohlbrecher, J.; Müller, E.; Schweizer, T.; Textor, M.; Reimhult, E. Triggered Release from Liposomes through Magnetic Actuation of Iron Oxide Nanoparticle Containing Membranes. *Nano Lett.* **2011**, *11*, 1664–1670.
- (16) Ang, K. L.; Venkatraman, S.; Ramanujan, R. V. Magnetic Pnipa Hydrogels for Hyperthermia Applications in Cancer Therapy. *Mater. Sci. Eng., C* **2007**, *27*, 347–351.
- (17) Purushotham, S.; Chang, P. E. J.; Rumpel, H.; Kee, I. H. C.; Ng, R. T. H.; Chow, P. K. H.; Tan, C. K.; Ramanujan, R. V. Thermoresponsive Core–Shell Magnetic Nanoparticles for Combined Modalities of Cancer Therapy. *Nanotechnology* **2009**, *20*, 305101.
- (18) Polo-Corrales, L.; Rinaldi, C. Monitoring Iron Oxide Nanoparticle Surface Temperature in an Alternating Magnetic Field Using Thermoresponsive Fluorescent Polymers. *J. Appl. Phys.* **2012**, *111*, 07B334.
- (19) Balasubramaniam, S.; Pothayee, N.; Lin, Y.; House, M.; Woodward, R. C.; St. Pierre, T. G.; Davis, R. M.; Riffle, J. S. Poly(N-Isopropylacrylamide)-Coated Superparamagnetic Iron Oxide Nanoparticles: Relaxometric and Fluorescence Behavior Correlate to Temperature-Dependent Aggregation. *Chem. Mater.* **2011**, *23*, 3348–3356.
- (20) Wang, Z.; Ma, X.; Zong, S.; Wang, Y.; Chen, H.; Cui, Y. Preparation of a Magneto-fluorescent Nano-Thermometer and Its Targeted Temperature Sensing Applications in Living Cells. *Talanta* **2015**, *131*, 259–265.
- (21) Hannecart, A.; Stanicki, D.; Vander Elst, L.; Muller, R. N.; Lecommandoux, S.; Thevenot, J.; Bonduelle, C.; Trotter, A.; Massot, P.; Miraux, S.; Sandre, O.; Laurent, S. Nano-Thermometers with Thermo-Sensitive Polymer Grafted Uspios Behaving as Positive Contrast Agents in Low-Field MRI. *Nanoscale* **2015**, *7*, 3754–3767.
- (22) Regmi, R.; Bhattacharai, S. R.; Sudakar, C.; Wani, A. S.; Cunningham, R.; Vaishnav, P. P.; Naik, R.; Oupicky, D.; Lawes, G. Hyperthermia Controlled Rapid Drug Release from Thermosensitive Magnetic Micogels. *J. Mater. Chem.* **2010**, *20*, 6158–6163.
- (23) Herrera, A. P.; Rodriguez, M.; Torres-Lugo, M.; Rinaldi, C. Multifunctional Magnetite Nanoparticles Coated with Fluorescent Thermo-Responsive Polymeric Shells. *J. Mater. Chem.* **2008**, *18*, 855–858.
- (24) Eyiler, E.; Walters, K. B. Magnetic Iron Oxide Nanoparticles Grafted with Poly(Itaconic Acid)-Block-Poly(N-Isopropylacrylamide). *Colloids Surf., A* **2014**, *444*, 321–325.
- (25) Frimpong, R. A.; Hilt, J. Z. Poly(N-Isopropylacrylamide)-Based Hydrogel Coatings on Magnetite Nanoparticles Via Atom Transfer Radical Polymerization. *Nanotechnology* **2008**, *19*, 175101.
- (26) Narain, R.; Gonzales, M.; Hoffman, A. S.; Stayton, P. S.; Krishnan, K. M. Synthesis of Monodisperse Biotinylated P(NipaaM)-Coated Iron Oxide Magnetic Nanoparticles and Their Bioconjugation to Streptavidin. *Langmuir* **2007**, *23*, 6299–6304.
- (27) Mu, B.; Wang, T.; Wu, Z.; Shi, H.; Xue, D.; Liu, P. Fabrication of Functional Block Copolymer Grafted Superparamagnetic Nanoparticles for Targeted and Controlled Drug Delivery. *Colloids Surf., A* **2011**, *375*, 163–168.
- (28) Lien, Y.-H.; Wu, T.-M. Preparation and Characterization of Thermosensitive Polymers Grafted onto Silica-Coated Iron Oxide Nanoparticles. *J. Colloid Interface Sci.* **2008**, *326*, 517–521.

- (29) Zirbs, R.; Lassenberger, A.; Vonderhaid, I.; Kurzhals, S.; Reimhult, E. Melt-Grafting for the Synthesis of Core–Shell Nanoparticles with Ultra-High Dispersant Density. *Nanoscale* **2015**, *7*, 11216–11225.
- (30) Binder, W. H.; Gloger, D.; Weinstabl, H.; Allmaier, G.; Pittenauer, E. Telechelic Poly(N-Isopropylacrylamides) Via Nitroxide-Mediated Controlled Polymerization and “Click” Chemistry: Livingness and “Grafting-from” Methodology. *Macromolecules* **2007**, *40*, 3097–3107.
- (31) Gong, Z.-l.; Tang, D.-y.; Guo, Y.-d. The Fabrication and Self-Flocculation Effect of Hybrid TiO_2 Nanoparticles Grafted with Poly(N-Isopropylacrylamide) at Ambient Temperature Via Surface-Initiated Atom Transfer Radical Polymerization. *J. Mater. Chem.* **2012**, *22*, 16872–16879.
- (32) Shi, Y.; Selin, V.; Wang, Y.; Sukhishvili, S. A. Multiresponsive Block Copolymer-Modified “Hairy” Gold Nanoparticles for Remote Control of Interfaces. *Part. Part. Syst. Char.* **2013**, *30*, 950–957.
- (33) Tan, L.; Liu, J.; Zhou, W.; Wei, J.; Peng, Z. A Novel Thermal and pH Responsive Drug Delivery System Based on $ZnO@Pnipam$ Hybrid Nanoparticles. *Mater. Sci. Eng., C* **2014**, *45*, 524–529.
- (34) Wang, S.; Zhou, Y.; Sun, W. Preparation and Characterization of Antifouling Thermosensitive Magnetic Nanoparticles for Applications in Biomedicine. *Mater. Sci. Eng., C* **2009**, *29*, 1196–1200.
- (35) Wu, T.; Zhang, Y.; Wang, X.; Liu, S. Fabrication of Hybrid Silica Nanoparticles Densely Grafted with Thermoresponsive Poly(N-Isopropylacrylamide) Brushes of Controlled Thickness Via Surface-Initiated Atom Transfer Radical Polymerization. *Chem. Mater.* **2008**, *20*, 101–109.
- (36) Li, D.; Cui, Y.; Wang, K.; He, Q.; Yan, X.; Li, J. Thermosensitive Nanostructures Comprising Gold Nanoparticles Grafted with Block Copolymers. *Adv. Funct. Mater.* **2007**, *17*, 3134–3140.
- (37) Li, D.; He, Q.; Cui, Y.; Wang, K.; Zhang, X.; Li, J. Thermosensitive Copolymer Networks Modify Gold Nanoparticles for Nanocomposite Entrapment. *Chem. - Eur. J.* **2007**, *13*, 2224–2229.
- (38) Ohno, K.; Ma, Y.; Huang, Y.; Mori, C.; Yahata, Y.; Tsujii, Y.; Maschmeyer, T.; Moraes, J.; Perrier, S. Surface-Initiated Reversible Addition–Fragmentation Chain Transfer (Raft) Polymerization from Fine Particles Functionalized with Trithiocarbonates. *Macromolecules* **2011**, *44*, 8944–8953.
- (39) Majewski, A. P.; Schallon, A.; Jérôme, V.; Freitag, R.; Müller, A. H. E.; Schmalz, H. Dual-Responsive Magnetic Core–Shell Nanoparticles for Nonviral Gene Delivery and Cell Separation. *Biomacromolecules* **2012**, *13*, 857–866.
- (40) Kakwani, H.; Leal, M. P.; Materia, M. E.; Curcio, A.; Guardia, P.; Niculae, D.; Marotta, R.; Falqui, A.; Pellegrino, T. Functionalization of Strongly Interacting Magnetic Nanocubes with (Thermo)-Responsive Coating and Their Application in Hyperthermia and Heat-Triggered Drug Delivery. *ACS Appl. Mater. Interfaces* **2015**, *7*, 10132–10145.
- (41) Davis, K.; Qi, B.; Witmer, M.; Kitchens, C. L.; Powell, B. A.; Mefford, O. T. Quantitative Measurement of Ligand Exchange on Iron Oxides Via Radio Labeled Oleic Acid. *Langmuir* **2014**, *30*, 10918–10925.
- (42) Grünwald, T. A.; Lassenberger, A.; van Oostrum, P. D. J.; Rennhofer, H.; Zirbs, R.; Capone, B.; Vonderhaid, I.; Amenitsch, H.; Lichtenegger, H. C.; Reimhult, E. Core–Shell Structure of Monodisperse Poly(Ethylene Glycol)-Grafted Iron Oxide Nanoparticles Studied by Small-Angle X-Ray Scattering. *Chem. Mater.* **2015**, *27*, 4763–4771.
- (43) Amstad, E.; Gillich, T.; Bilecka, I.; Textor, M.; Reimhult, E. Ultrastable Iron Oxide Nanoparticle Colloidal Suspensions Using Dispersants with Catechol-Derived Anchor Groups. *Nano Lett.* **2009**, *9*, 4042–4048.
- (44) Hyeon, T.; Lee, S. S.; Park, J.; Chung, Y.; Na, H. B. Synthesis of Highly Crystalline and Monodisperse Maghemite Nanocrystallites without a Size-Selection Process. *J. Am. Chem. Soc.* **2001**, *123*, 12798–12801.
- (45) Mondini, S.; Ferretti, A. M.; Puglisi, A.; Ponti, A. Pebbles and Pebblejuggler: Software for Accurate, Unbiased, and Fast Measurement and Analysis of Nanoparticle Morphology from Transmission Electron Microscopy (TEM) Micrographs. *Nanoscale* **2012**, *4*, 5356–5372.
- (46) Ye, J.; Narain, R. Water-Assisted Atom Transfer Radical Polymerization of N-Isopropylacrylamide: Nature of Solvent and Temperature. *J. Phys. Chem. B* **2009**, *113*, 676–681.
- (47) Klein Gunnewiek, M.; Di Luca, A.; Sui, X.; van Blitterswijk, C. A.; Moroni, L.; Vancso, G. J. Controlled Surface Initiated Polymerization of N-Isopropylacrylamide from Polycaprolactone Substrates for Regulating Cell Attachment and Detachment. *Isr. J. Chem.* **2012**, *52*, 339–346.
- (48) Li, D.; Zhang, X.; Yao, J.; Simon, G. P.; Wang, H. Stimuli-Responsive Polymer Hydrogels as a New Class of Draw Agent for Forward Osmosis Desalination. *Chem. Commun.* **2011**, *47*, 1710–1712.
- (49) Mahdavi, M.; Ahmad, M.; Haron, M.; Namvar, F.; Nadi, B.; Rahman, M.; Amin, J. Synthesis, Surface Modification and Characterisation of Biocompatible Magnetic Iron Oxide Nanoparticles for Biomedical Applications. *Molecules* **2013**, *18*, 7533–7548.
- (50) Montagne, F.; Mondain-Monval, O.; Pichot, C.; Mozzanega, H.; Eläissari, A. Preparation and Characterization of Narrow Sized (O/W) Magnetic Emulsion. *J. Magn. Magn. Mater.* **2002**, *250*, 302–312.
- (51) Beyler, C. L.; Hirschler, M. M. Thermal Decomposition of Polymers. In *SFPE Handbook of Fire Protection Engineering*, 3rd ed.; DiNenno, P. J., Ed.; National Fire Protection Association: Quincy, MA, 2001.
- (52) Bixner, O.; Lassenberger, A.; Baurecht, D.; Reimhult, E. Complete Exchange of Hydrophobic Dispersant Shell on Monodisperse Superparamagnetic Iron Oxide Nanoparticles. *Langmuir* **2015**, [in press], DOI: [10.1021/acs.langmuir.5b01833](https://doi.org/10.1021/acs.langmuir.5b01833).
- (53) Motornov, M.; Sheparovich, R.; Lupitskyy, R.; MacWilliams, E.; Minko, S. Responsive Colloidal Systems: Reversible Aggregation and Fabrication of Superhydrophobic Surfaces. *J. Colloid Interface Sci.* **2007**, *310*, 481–488.
- (54) Lo Verso, F.; Egorov, S. A.; Milchev, A.; Binder, K. Spherical Polymer Brushes under Good Solvent Conditions: Molecular Dynamics Results Compared to Density Functional Theory. *J. Chem. Phys.* **2010**, *133*, 184901.
- (55) Dionigi, C.; Pineiro, Y.; Riminiucci, A.; Banobre, M.; Rivas, J.; Dedi, V. Regulating the Thermal Response of Pnipam Hydrogels by Controlling the Adsorption of Magnetite Nanoparticles. *Appl. Phys. A: Mater. Sci. Process.* **2014**, *114*, 585–590.
- (56) Dionigi, C.; Lungaro, L.; Goranov, V.; Riminiucci, A.; Pineiro-Redondo, Y.; Banobre-Lopez, M.; Rivas, J.; Dedi, V. Smart Magnetic Poly(N-Isopropylacrylamide) to Control the Release of Bio-Active Molecules. *J. Mater. Sci.: Mater. Med.* **2014**, *25*, 2365–2371.
- (57) Schönhoff, M.; Larsson, A.; Welzel, P. B.; Kuckling, D. Thermoreversible Polymers Adsorbed to Colloidal Silica: A ^{1}H NMR and DSC Study of the Phase Transition in Confined Geometry. *J. Phys. Chem. B* **2002**, *106*, 7800–7808.
- (58) Wakamatsu, H.; Yamamoto, K.; Nakao, A.; Aoyagi, T. Preparation and Characterization of Temperature-Responsive Magnetite Nanoparticles Conjugated with N-Isopropylacrylamide-Based Functional Copolymer. *J. Magn. Magn. Mater.* **2006**, *302*, 327–333.